Marí, B.; Singh, KC.; Verma, N. (2016). Optical properties of Yb3+ doped ZnO/MgO nanocomposites. Ceramics International. 42(11):13018-13023. doi:10.1016/j.ceramint.2016.05.079.

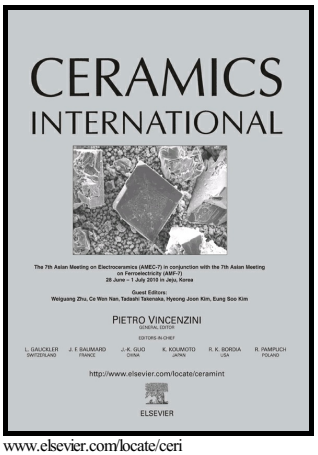

www.elsevier.com/locate/ceri

Optical properties of Yb-doped ZnO/MgO nanocomposites

B. Marí, K.C. Singh, N. Verma, J. Jindal

PII: S0272-8842(16)30684-8
DOI: http://dx.doi.org/10.1016/j.ceramint.2016.05.079
Reference: CERI12884

To appear in: *Ceramics International*

Received date: 31 March 2016
Accepted date: 13 May 2016

Cite this article as: B. Marí, K.C. Singh, N. Verma and J. Jindal, Optica properties of Yb-doped ZnO/MgO nanocomposites, *Ceramics Internationa* http://dx.doi.org/10.1016/j.ceramint.2016.05.079

Optical properties of Yb-doped ZnO/MgO nanocomposites

B. María[a], K. C. Singh[b] N. Verma[b], J. Jindal[b]

[a] Institut de Disseny per la Fabricació Automatitzada (IDF) - Departament de Física Aplicada, Universitat Politècnica de València, Camí de Vera s/n, 46022 València, Spain

[b] Department of Chemistry, Maharshi Dayanand University, Rohtak 124001, Haryana, India

Abstract:

Yb^{3+} doped ZnO/MgO nanocomposite were prepared by combustion synthesis method. The samples were further heated to 1000 ºC to improve their crystallinity and photoluminescent efficiency. The concentrations of Yb^{3+} and Mg^{2+} were varied between 1 to 2% and 5 to 70% respectively in prepared samples. The nano-powders were characterized by Scanning Electron Microscopy and X Ray Diffraction for morphology and structural determination. XRD studies have revealed the wurtzite structure for $Mg_xZn_{1-x}O$ for Mg concentrations below 30 %. Higher concentrations of Mg results in Yb^{3+} doped ZnO/MgO nanocomposite containing three phases; the wurzite hexagonal phase typical of ZnO, the cubic phase of MgO and a small amount of cubic Yb_2O_3 phase. As expected, the amount of cubic phase in nano-powders increased with the increase of Mg concentration in ZnO. The crystallite size of ZnO/MgO composites decreased from 55 nm to 30 nm with increase of Mg content. SEM images of Yb^{3+} doped ZnO/MgO nanocomposite with higher Mg content (> 50%) showed clearly distinct hexagonal and cubical shaped nano-particles. Photoluminescent emission showed a broad band in the range (435 nm to 700 nm). Pure ZnO nano-phosphor showed an emission peak around 545 nm, which is blue shifted with Mg content. The photoluminescence intensity increased with increase of Mg content in ZnO and it became maximum with 30% Mg concentration. Time resolved decay curves of photoluminescence indicated decay time in microsecond time scale.

Keywords: ZnMgO, Yb doping, Combustion method, Photoluminescence, Nanocomposites.

1. Introduction

ZnO is a versatile material and used widely as a semiconductor with a wide band gap of 3.3 eV at room temperature. ZnO has numerous applications in many fields like solar cells, piezoelectric transducers, phosphors, chemical and gas sensors. In a wide gap semiconductor, the addition of anionic or cationic impurities often induces appreciable changes in its electrical and optical properties. Various ZnO nanostructures doped with different elements (e g. Al, Ga, In, Co, Sb) has been synthesized by several investigators [1-4]. The band gap energy of ZnO can be further increased by doping with Mg^{2+} to produce a ternary semiconductor like $Mg_xZn_{1-x}O$ or a mixed oxide as ZnO/MgO [5]. Since the atomic radii of Zn^{2+} (0.6 Å) and Mg^{2+} (0.57 Å) are similar [6], the substitution between these two atoms in the structure does not change the lattice constant of $Mg_xZn_{1-x}O$ significantly but causes a substantial change in optical and electronic properties of ZnO. In addition, the crystal defect structure of ZnO can be minimized by doping with Mg^{2+} [7].

However, fabrication of $Mg_xZn_{1-x}O$ is practically limited because of the demarcated solubility of MgO in ZnO. On the basis of the phase diagram of ZnO and MgO binary systems, the thermodynamic solid solubility of MgO in ZnO is less than 4% since the crystal structure of MgO (cubic, a = 4.24 Å) and ZnO (hexagonal wurtzite, a = 3.24 Å and c = 5.20 Å) are different [8, 9]. The production of an enlarged band gap in $Mg_xZn_{1-x}O$ with the replacement of Zn^{2+} species with Mg^{2+} has however been achieved by some groups using a variety of techniques including pulsed laser deposition (PLD), molecular-beam epitaxy (MBE), metalorganic vapor-phase epitaxy (MOVPE), magnetron sputtering, sol–gel, chemical vapor deposition, and electron beam evaporation [10-13].

Up to 33% of Mg solubility in ZnO has been reported in reference [14]. The Mg doping can be increased further and up to 67% at high temperature and pressure [15]. It has been predicted that the high temperature microwave assisted combustion route leads to a wurtzite phase even for a large Mg

concentration (80 %) in ZnO samples [16]. Mg doped ZnO nanostructures have been prepared by various methods i.e. nanowires, ZnO/MgZnO quantum wells by PLD [17-18], nanorods, nanowires and dendritic nanostructure by thermal evaporation [19-20]. Red luminescence is produced when ZnO is doped with Li, Na, Bi or Cu [21-22]. However, no attempts have been made to fabricate nanocrystallites of the mixed oxides $Mg_xZn_{1-x}O$ doped with Yb^{3+} to observe the down conversion or down shifting property due to Yb^{3+} at about 980 nm. It is expected that a thin layer of this material over solar cell will enhance the conversion efficiency of the cell.

In the present work, we report on a simple approach to develop tuned band gap $Mg_xZn_{1-x}O$: Yb^{3+} nano-powders with different Mg^{2+} content via combustion synthesis method. The combustion synthesis method had been earlier used by us to prepare phosphor materials consisting of ZrO_2, $BaZrO_3$ and MLn_2O_4 (M=Ba or Sr, Ln=Gd or La) doped with Eu^{3+} and Tb^{3+} ions [23, 24]. This method provides an interesting alternative over other elaborated techniques because it offers several attractive advantages such as: simplicity of experimental set-up; surprisingly short time between the preparation of reactants and the availability of the final product; and being cheap due to energy saving. The main point of this method is the rapid decomposition of the rare earth nitrate in the presence of an organic fuel. During the reaction, many gases, such as CO_2, N_2, NO_2 and H_2O as well as a large amount of heat are released in a short period of time before the process terminates with white, foamy and crisp products. Many times final products are found to be composed of nanosized particles [25].

A systematic study of the effect of Mg^{2+} and Yb^{3+} content on morphology, crystalline microstructure, and optical properties on $Mg_xZn_{1-x-y}O$: Yb_y^{3+} nano-powders are investigated by using various analytical techniques. The results from this investigation show that $Mg_xZn_{1-x-y}O$: Yb_y^{3+} nanocrytallites exhibit higher crystalline defect structures than ZnO nanocrystallites and enhanced optical properties,

rendering them as promising nanostructured materials for potential use in optoelectronic devices. The effect of ytterbium doping in $Mg_xZn_{1-x}O$ phosphor has also been analyzed.

2. EXPERIMENTAL

High purity [Mg $(NO_3)_2$], [Zn $(NO_3)_2$], [Yb $(NO_3)_3$] and urea from Sigma Aldrich were used as starting material. The calculated amount for the formation of $Mg_{(x)}$ $Yb_{(y)}$: $Zn_{(1-x-y)}$ O: complex were taken and mixed with a calculated amount of urea and a paste material was prepared. The paste of mixture was transferred to preheated furnace at 600 ºC. The urea amount was calculated using total oxidizing reducing valences [25]. At high temperature the material undergoes rapid dehydration, combustion and a voluminous solid is formed with the generation of combustible gases. The solid obtained is again annealed at 1000 ºC for 3 h to increase the crystalline character.

The morphology of the crystals was studied by scanning electron microscope (SEM) using JEOL JSM6300 model operating at 10 kV. Photoluminescence (PL) experiments were performed in backscattering geometry using a He–Cd laser (325 nm) with an optical power of 30 mW for excitation. The emitted light was analyzed by HR-4000 Ocean Optics USB spectrometer optimized for the UV–Vis range. For photoluminescence measurements and decay lifetimes, 0.05 g powder samples were pressed into pellets (10 mm diameter and 1 mm thickness) and then exposed to a 325 nm He-Cd laser. All measurements were carried out at room temperature. The structural characterization was performed by high resolution X-ray diffraction (XRD) using Rigaku Ultima IV diffractometer in the θ–2θ configuration and using Cu Kα radiation (1.54184 Å).

3. Result and Discussion

3.1 XRD studies

XRD patterns of Yb^{3+} doped ZnO/MgO nanocomposites synthesized by combustion method at 600 ºC and further annealed for three hours at 1000 °C are shown in Fig. 1a, which shows the presence of wurtzite ZnO peaks, cubic MgO peaks and also Yb_2O_3 peaks in the detection limit. The crystallite size of the Yb^{3+} doped ZnO/MgO composites was estimated by Scherrer equation to be ~29–53 nm. The crystallite size decreases with the increase of Mg content (Fig. 1b), but not in a regular manner. For the samples prepared with 20% Mg or more, ZnO and MgO phases were clearly identified by the presence of wurtzite ZnO (1 0 1), (1 0 0), (0 0 2) [JCPDS Card No. 36-1451] and cubic MgO (1 1 1), (2 0 0), (2 2 0) [JCPDS Card No. 4-0829] and Yb_2O_3 diffraction peaks [JCPDS Card No.00-041-1106]. The peaks due to Yb_2O_3 phase are very small but definite. This fact indicates that the synthesized product was not a single phase but a composite. Strong evidence of incorporation of MgO in ZnO phase, however, comes from the fact that (0 0 2) XRD peak shifted to higher angles (2θ) from 34.43 for ZnO to 34.63 (Fig. 1c) for ZnO/MgO composite (70 mol% Mg). This indicates shortening of c-axis length by 0.58%, as also reported by many authors due to incorporation of Mg in wurtzite ZnMgO lattice [26-30]. Small change in lattice parameter is probably due to similar ionic radius of Zn^{2+} (0.60 Å) and Mg^{2+} (0.57 Å). Energy Dispersive X-ray Analysis (EDAX) of Yb^{3+} doped ZnO/MgO nanocomposites (Table 1) shows that the samples having > 10% Mg doping are deficient in Zn. The results not only indicate incorporation of Mg in ZnO lattice but also the manifestation of the high vapour pressure of Zn at high temperature [2, 30-31]. Zinc evaporation happens at temperatures exceeding 400 °C as melting point of zinc is 419 °C and zinc can be desorbed more easily than Mg at high growth temperature. Hence, from EDAX and XRD results, we can say that the prepared samples are ZnMgO alloy with some segregated cubic MgO phase at higher Mg concentration. The presence of Yb_2O_3 phase in all ZnO/MgO

composites indicates the difficult incorporation of even 1% Yb^{3+} in ZnO phase. Photoluminescence studies have also confirmed the same fact (Section 3.3).

3.2 SEM micrograph analysis

A representative SEM micrographs of Yb^{3+} doped ZnO/MgO composite with 5, 10, 20, 30, 50 and 70% Mg is shown in Fig. 2. It shows that the particles with low Mg content have severe aggregation but still appear to be hexagonal, ellipsoid and spherical in shape on an individual basis. The particle size of samples increases with the increase of Mg content. The sample 5e and 5f have larger particle size with distinct hexagonal and cubical shaped morphology with good crystalline quality.

3.3 Photoluminescence properties

The PL spectra of ZnO/MgO nanocomposites doped with Yb (1% or 2%) were measured with a U .V. excitation source of 325 nm and are presented in Fig. 3 a, b. All the samples with different compositions of Mg from 5% to 70% show a broad visible luminescence band. The intensity of band is maximum for ZnO/MgO (30% Mg, 1% Yb). The undoped ZnO shows a broad band at band maximum 545 nm. When Mg (5%) and Yb (1%) are doped in ZnO there is a blue shift in the emission band and the band maximum shifted from 545 to 516 nm. Further increase of Mg content results in a gradual red shift of PL peak, which shifts from 532 nm in ZnO/MgO (20% Mg, 1% Yb) to 538 nm in ZnO/MgO (30% to 70% Mg, 1% Yb). The PL spectrum of pure ZnO is related to the intrinsic defect in ZnO crystal. During the synthesis of material some defects, such as oxygen vacancies or interstitial zinc or zinc vacancies may appear in the lattice, which is the origin of visible emission [32-33]. As EDAX analysis has shown that Yb^{3+} doped ZnO/MgO nanocomposites samples with 5% and 10% Mg are deficient in oxygen content, some defects such as oxygen vacancies (V_0) or interstitial zinc (Zn_i) may appear in the samples, but nanocomposites having Mg content >10% are deficient in zinc hence many zinc vacancies (V_{Zn}) exist in nanocomposites and they can act as acceptor centres. The transition of an

electron from the conduction band or a shallow level close to conduction band to an empty state in V_{Zn} or defect level about 2 eV below the conduction band would give rise to visible emission in ZnO/MgO nano composite. This shallow donor may be Zn or Mg in interstitial position. The position of emission peak in oxygen deficient samples shifts to a shorter wavelength (516 nm) and it is gradually red shifted with Zn deficient samples (539 nm). It is the manifestation of the fact that the separation between defect levels in oxygen deficient samples is more than that of Zn deficient composites. As Mg content is more than stoichiometric amount of Mg, in Zn deficient composites, interstitial Mg (Mg_i) might be forming shallow donor states. In pure ZnO, green emission at 545 nm is mostly believed to arise from oxygen vacancy related defect centres. One possible mechanism could be recombination between Zn_i and oxygen vacancy/antisite oxygen. As Zn_i is fewer in number, PL intensity is very small. In Yb^{3+} doped ZnO/MgO nanocomposites, as number of Mg_i defect increases, intensity of emission increases due to Mg_i/V_{Zn} recombination. The process reaches its optimum value in 30 mol% Mg above which MgO phase probably separates. PL emission characteristics for 50 and 70 mol% Mg in ZnO/MgO nanocomposites, remain the same but with diminished intensity as can be seen from Fig. 3a. Gaussian fitting results of PL spectra of $Mg_{0.30}$ $Zn_{0.69}Yb_{0.01}O$ composition are shown in Fig. 3c. The PL band shows three peaks situated at 507, 553, 592 nm. These three peaks are attributed to oxygen vacancies in ZnO crystal lattice [34]. The oxygen vacancies are influenced by the particle size. When the particles size increases the surface defects are reduced due to decrease in surface area. Thus photoluminescence decreases. This may have happened in the compositions $Mg_{0.50}$ $Zn_{0.49}Yb_{0.01}$ O and $Mg_{0.70}$ $ZnO_{0.29}Yb_{0.01}O$ because their particles size are bigger than the other compositions (Fig. 2 e, f) so the intensity of these compositions are very low. The other reason for decrease in photoluminescence intensity with increase in Mg content could be the formation of heterojunction of ZnO/MgO [35].

It may be observed from Fig. 3b that increase of Yb^{3+} doping has little effect on the position of emission band but it affects PL intensity. 5% Mg doping in ZnO causes increase of PL intensity with blue shift. 1% Yb with 5% Mg doping in ZnO enhances PL emission but it decreases to half with 2% Yb doping. Probable reason may be the increase of defects with introduction of trivalent Yb in place of bivalent zinc. At least one defect will be created in the lattice with the introduction of a Yb^{3+} in place of Zn^{2+}, but the 2% Yb doping seems to causing concentration quenching or radiation less recombination of defects.

It has been shown [36, 37] that Yb^{3+} doped ZnO in glass and glass ceramics, an emission band near 1000 nm coming from the Yb^{3+}: $^2F_{5/2} \rightarrow {}^2F_{7/2}$ transition and an intense blue emission band ranging from 300 to 500 nm related to ZnO defect are observed. Moreover, the excitation bands of the blue emission overlapped with the excitation bands of Yb^{3+}, giving the evidences of energy transfer between the ZnO-related defects to Yb^{3+}. In the glass ceramic containing ZnO nanocrystals, the excitation bands of Yb^{3+} were located at near-UV-blue region, with peak at 390 nm. Excited by 390 nm, intense yellow emission at about 590 nm and near-IR emission around 1000 nm of Yb^{3+} were observed. The yellow emission, involved in the recombination of the excited electrons and deeply trapped holes, was usually obtained in ZnO crystals or films that were prepared under oxygen-rich conditions [38-40]. Similar energy transfer between ZnO and Yb^{3+} has been reported in ZnO-$LiYbO_2$ phosphor [41], in which Li^+ related defects enabled higher energy transfer efficiency between ZnO and Yb^{3+}. We were also expecting similar behavior of energy transfer in Yb^{3+} doped ZnO/MgO nanocomposites to obtain an intense peak near 1000 nm corresponding to Yb^{3+}: $^2F_{5/2} \rightarrow {}^2F_{7/2}$ transition. Of course a weak emission peak in $Mg_{0.05}Zn_{0.94}O:Yb^{3+}{}_{0.01}$ nanocomposite (Fig. 3b) confirms the energy transfer from ZnO/MgO lattice defects transitions to Yb^{3+}: $^2F_{5/2} \rightarrow {}^2F_{7/2}$ transition. But its low conversion efficiency put a question mark to use them as a down-conversion material in solar cells. Absence of emission peak near IR

region in other Yb^{3+} doped ZnO/MgO compositions with Mg>5% and Yb>1% doping indicate interference of Mg^{2+} and Yb^{3+} for efficient energy transfer.

The decay curves for Yb^{3+} doped ZnO/MgO nanocomposites are shown in Fig. 4. The decay curves clearly showed that the decay time of Yb^{3+} doped ZnO/MgO nanocomposites with 1% Yb and 10, 20, 30 % Mg concentration (Samples labelled as B4A, B5A and B6A in Table 1 and Figure 4) is almost same and it is in the range of milliseconds. The decay curves could be fitted in to single exponential decay. The time resolved decay measurements suggested that the photophysical processes in ZnO/MgO nanocomposites include excitation of charge carriers followed by redistribution in trap states and subsequent recombination in time scale of tens to hundreds of μs (Fig. 4). The measured luminescence decay times for the measured samples are in the range 93-125 microseconds as displayed in the inset of Fig. 4.

Conclusion

Yb^{3+} (1% or 2%) doped ZnO/MgO nanocomposites up to 70% Mg were prepared by combustion synthesis method. XRD studies reveal the presence of wurtzite structure of $Mg_xZn_{1-x}O$ phase below 30% Mg concentrations. Higher concentrations of Mg results in several crystalline phases in Yb^{3+} doped ZnO/MgO nanocomposites with the wurzite phase of ZnO, the cubic phase of MgO and a small amount of cubic phase of Yb_2O_3. The crystallite size of ZnO/MgO composites decreased from 55 nm to 30 nm with increase of Mg content. SEM images of Yb^{3+} doped ZnO/MgO nanocomposites with higher Mg content (> 50%) showed clearly distinct hexagonal and cubical shaped nanoparticles with larger size and a good crystalline quality.

Photoluminescent green emission in Yb^{3+} doped ZnO/MgO nanocomposites increases up to 30% with Mg doping, then there is a gradual decrease of intensity with increase of Mg concentration. This fact has been assigned to the segregation of Mg over the ZnO particles. Oxygen deficient Yb^{3+} doped

ZnO/MgO nanocomposites are blue shifted to greater extent than that of Zn deficient composites. The enhancement of luminescence is also associated with a fast decay component, which could be due to large number of traps created in the high Mg (up to 30%) ratio nanocomposites. A weak emission peak in $Mg_{0.05}Zn_{0.94}O:Yb^{3+}_{0.01}$ nanocomposite confirms the energy transfer from ZnO/MgO lattice defects transitions to Yb^{3+}: $^2F_{5/2} \rightarrow {}^2F_{7/2}$ transition. But its low conversion efficiency put a question mark to use them as a down-conversion material in solar cells.

Acknowledgments

This work was supported by Ministerio de Economía y Competitividad (ENE2013-46624-C4-4-R), Generalitat Valenciana (PROMETEUS-II/2014/044) and the European Commission through NanoCIS project (FP7-PEOPLE-2010-IRSES ref. 269279).

References

1. Jung SW, Park WI, Yi GC, Kim MY (2003) Fabrication and Controlled Magnetic Properties of Ni/ZnO Nanorod Heterostructures. Adv. Mater, 15: 1358-1361. doi: 10.1002/adma.200305172
2. Jie J, Wang G, Han X, Yu Q, Liao Y, Li G, Hou JG (2004) Indium-doped zinc oxide nanobelts. Chem Phys Lett 387:466-470. doi:10.1016/j.cplett.2004.02.045
3. Yan M, Zhang HT, Widjaja EJ, Chang RPH (2003) Self-assembly of well-aligned gallium-doped zinc oxide nanorods. J. Appl. Phys. 94:5240-5246. doi: 10.1063/1.1608473
4. Chen H, Qi J, Huang Y, Liao Q, Zhang Y (2007) Synthesis, Structure and Properties of Sn-doped ZnO Nanobelts. Acta Physico-Chimica Sinica 23:55-58. doi:10.1016/S1872-1508(07)60005-9
5. Shan FK, Kim BI, Liu GX, Liu ZF, Sohn JY, Lee WJ, Shin BC, Yu YS (2004) Blueshift of near band edge emission in Mg doped ZnO thin films and aging. J. Appl. Phys. 95:4772-4776. doi: 10.1063/1.1690091
6. A. R. West, solid state Chemistry, John Wiley and Sons, 1987.
7. Tomar MS, Melgarejo Dobal PS, Katiyar RS (2001) Synthesis of Zn_{1-}xMgxO and its structural characterization. J. Mater. Res. 16:903-906. doi: http://dx.doi.org/10.1557/JMR .2001.0127
8. Bhattacharya P, Das RR, Katiyar RS (2003) Fabrication of stable wide-band-gap ZnO/MgO multilayer thin films. Appl. Phys. Lett. 83:2010-2012. doi: 10.1063/1.1609250
9. Xue M, Guo Q, Wu K, Guo J (2008) Tunable surface band gap in MgxZn1−xO thin films. J. Chem. Phys.129:234707-234712. doi: 10.1063/1.3041774
10. Aykut Y, Parsons GN, Pourdeyhimi B, Khan SA (2013) Synthesis of mixed ceramic Mg_xZn_{1-x} nanofibres via Mg^{2+} Doping using sol gel Electrospinning. Langmuir 29:4159-4166. doi: 10.1021/la400281c
11. Jin YB, Zhang B, Yang SM, Wang YZ, Chen J, Zhang H, Huang C, Cao C, Chang RPH (2001) Room temperature UV emission of $Mg_xZn_{1-x}O$ films Solid State Commun. 119:409-413. doi:10.1016/S0038-1098(01)00244-7
12. Li J, Huang JH, Song WJ, Tan RQ, Yang Y, Li XM (2010) Effect of deposition ambient on structural and optical properties of $Mg_xZn_{1-x}O$ alloy thin films grown by RF sputtering. J. Mater Sci.: Mater. Electron. 21:1327-1331. doi 10.1007/s10854-010-0070-6
13. Chen NB, Sui CH (2006) Recent progress in research on $Mg_xZn_{1-x}O$ alloys Mater. Sci. Eng. B 126:16– 21.

14. Park WI, Chul Yi G, Jang HM (2001) Metalorganic vapor-phase epitaxial growth and photoluminescent properties of Zn1−xMgxO(0⩽x⩽0.49) thin films. Appl. Phys. Lett. 79:2022-2024. doi: 10.1063/1.1405811
15. Sharma AK, Narayan J, Muth JF, Teng CW, Jin C, Kvit A, Kolbas RM, Holland OW (1999) Optical and structural properties of epitaxial Mg x Zn 1−x O alloys. Appl. Phys. Lett. 75:3327-3329. doi: 10.1063/1.125340
16. Sundar Manoharan S, Sonia (2009) Photoluminescent properties of Mg doped ZnO by microwave combustion and microwave polyol method. Material science and engineering B 162:68-73. doi:10.1016/j.mseb.2009.02.004
17. Rahm A, Nobis T, Lorenz M, Zimmermann G, Boukos N, Travlos A, Grundmann M (2007) Growth Evolution and Characterization of PLD Zn(Mg)O Nanowire Arrays. Advances in Solid State Physics 46:113-125.
18. Czekalla C, Guinard J, Hanisch C, Cao BQ, Kaidashev EM, Boukos N, Travlos A, Renard J, Gayral B, Dang DLS, Lorenz M, Grundmann M (2008) Spatial fluctuations of optical emission from single ZnO/MgZnO nanowire quantum wells Nanotechnology 19:115202-115207. doi:10.1088/0957-4484/19/11/115202
19. Ahn KS, Kang MS, Lee JK, Shin BC, Lee JW (2006) Enhanced electron diffusion length of mesoporous TiO2 film by using Nb2O5 energy barrier for dye-sensitized solar cells. Appl. Phys. Lett. 89:013103-013305. doi: 10.1063/1.2218831
20. Pan H, Zhu Y, Sun H, Feng Y, Sow CH, Lin J (2006) Electroluminescence and field emission of Mg-doped ZnO tetrapods. Nanotechnology 17:5096-5100. http://iopscience.iop.org/0957-4484/17/20/009
21. Pierce BJ, Hengehold RL (1976) Depth-resolved cathodoluminescence of ion-implanted layers in zinc oxide. J. appl. Phys. 47:644-651. doi: 10.1063/1.322627
22. Xu CX, Sun XW, Zhang XH, Ke L, Chua SJ (2004) Photoluminescent properties of copper-doped zinc oxide nanowires. Nano technology 15:856-861.
23. Marí B, Singh K, Sahal M, Khatkar S, Taxak V, Kumar M (2010) Preparation and luminescence properties of Tb^{3+} doped ZrO_2 and $BaZrO_3$ phosphors. J. Lumin. 130:2128-2132. doi:10.1016/j.jlumin.2010.06.005

24. Marí B, Singh KC, Cembrero-Coca P, Singh I, Singh D, Chand S (2013) Red emitting $MTiO_3$ (M = Ca or Sr) phosphors doped with Eu^{3+} or Pr^{3+} with some cations as co-dopants. Displays 34:346-351. doi:10.1016/j.displa.2013.07.003
25. Ekambaram S, Patil K (1997) Synthesis and properties of Eu^{2+} activated blue phosphors. J. Alloys Compd. 248:7-12. doi:10.1016/S0925-8388(96)02622-9
26. Ohtomo A, Kawasaki M, Koida T (1998) Mg x Zn 1−x O as a II–VI widegap semiconductor alloy. Appl. Phys. Lett. 72:2466-2468. doi: 10.1063/1.121384
27. Ogawa Y, Fujihara S (2002) Band-gap modification and tunable blue luminescence of wurtzite $MgxZn_{1-}xO$ thin films. Phys. Stat. Sol. 202:1825-1828. doi: 10.1002/pssa.200520053
28. Sharma AK, Narayan J, Muth JF, Teng CW, Jin C, Kvit A, Kolbas RM, Holland OW (1999) Optical and structural properties of epitaxial MgxZn1−xO alloys. Appl. Phys. Lett. 75:3327-3329. doi: 10.1063/1.125340
29. Park WI, Yi GC, Jang HM (2001) Metalorganic vapor-phase epitaxial growth and photoluminescent properties of Zn1−xMgxO(0⩽x⩽0.49) thin films. Appl. Phys. Lett. 79:2022-2024. doi: 10.1063/1.1405811
30. Kim JW, Kang HS, Kim JH, Lee SY (2006) Variation of structural, electrical, and optical properties of Zn1−xMgxO thin films. J. Appl. Phys.100:033701-033705. doi: 10.1063/1.2219153
31. Matsubara K, Tampo H, Yamada A, Fons P, Iwata K, Sakurai K, Niki S (2003) Bandgap Engineering of ZnO Transparent Conducting Films. Mater. Res. Soc. Symp. Proc. 763:B7.2.1. doi: http://dx.doi.org/10.1557
32. Heo YW, Norton DP, Pearton SJ (2005) Origin of green luminescence in ZnO thin film grown by molecular-beam epitaxy. J. Appl. Phys. 98:073502-073507. doi: 10.1063/1.2064308
33. Lin B, Fu Z, Jia Y (2001) Green luminescent center in undoped zinc oxide films deposited on silicon substrates. Appl. Phys. Lett., 79:943-945. doi: 10.1063/1.1394173
34. Mahamuni S, Borgohain K, Bendre BS, Leppert Valerie J, Risbud SH (1999) Spectroscopic and structural characterization of electrochemically grown ZnO quantum dots. J. appl. Phys. 85:2861-2865. doi: 10.1063/1.369049
35. Fu Z, Dong W, Yang B, Wang Z, Yang Y, Yan H, Zhang S, Zuo J, Ma M, Liu X (2006) Effect of MgO on the enhancement of ultraviolet photoluminescence in ZnO. Solid State Communication 138:179-183.

36. Luo Q, Qiao X, Fan X, Zhang X (2011) Near-infrared emission of Yb^{3+} through energy transfer from ZnO to Yb^{3+} in glass ceramic containing ZnO nanocrystals Optics Letters 36:2767-2769. http://dx.doi.org/10.1364/OL.36.002767
37. Qian GJ, Liang XL, Bei JF, Yuan SL, Chen GR (2007) Photoluminescence Properties of Zinc Oxide in Barium and Fluorine Silicate Glasses. J. Am. Ceram. Soc. 90:1255-1257. doi: 10.1111/j.1551-2916.2007.01594.x
38. Zeng XY, Yuan JL, Wang ZY, Zhang L (2007) Nanosheet-Based Microspheres of Eu^{3+}-doped ZnO with Efficient Energy Transfer from ZnO to Eu^{3+} at Room Temperature. Adv. Mater. 19:4510-4514. doi: 10.1002/adma.200602396
39. Studenikin SA, Golego N, Cocivera M (1998) Fabrication of green and orange photoluminescent, undoped ZnO films using spray pyrolysis. J. Appl. Phys. 84:2287-2294. doi: 10.1063/1.368295
40. Djurisic AB, Leung YH, Tam KH, Ding L, Ge WK, Chen HY, Gwo S (2006) Green, yellow, and orange defect emission from ZnO nanostructures: Influence of excitation wavelength. Appl. Phys. Lett. 88:103107-103109. doi: 10.1063/1.2182096
41. Ye S, Jiang N, He F, Liu X, Zhu B, Teng Y, Qiu JR (2010) Intense near-infrared emission from ZnO-$LiYbO_2$ hybrid phosphors through efficient energy transfer from ZnO to Yb^{3+}. Opt. Express 18:639-644.

FIGURE CAPTIONS

Fig. 1a. XRD pattern of Mg^{2+}: Yb^{3+}: ZnO nanophosphor powder (a) $Mg_{(5\%)}Yb_{(1\%)}$:ZnO, (b) $Mg_{(10\%)}Yb_{(1\%)}$:ZnO, (c) $Mg_{(20\%)}Yb_{(1\%)}$: ZnO, (d) $Mg_{(30\%)}Yb_{(1\%)}$:ZnO, (e) $Mg_{(50\%)}Yb_{(1\%)}$:ZnO, (f) $Mg_{(70\%)}Yb_{(1\%)}$:ZnO.

Fig. 1b. The variation of crystallite size in Yb^{3+} doped ZnO/MgO nanocomposites calculated from Scherrer equation.

Fig. 1c. Position of 002-diffraction peak of ZnO in Yb^{3+} doped ZnO/MgO nanocomposites.

Fig. 2. SEM images of Yb^{3+} doped ZnO/MgO nanocomposites: (a) $Mg_{(5\%)}Yb_{(1\%)}$:ZnO, (b) $Mg_{(10\%)}Yb_{(1\%)}$:ZnO, (c) $Mg_{(20\%)}Yb_{(1\%)}$: ZnO, (d) $Mg_{(30\%)}Yb_{(1\%)}$:ZnO, (e) $Mg_{(50\%)}Yb_{(1\%)}$:ZnO, (f) $Mg_{(70\%)}Yb_{(1\%)}$:ZnO.

Fig. 3a. PL emission spectra ZnO: Mg^{2+}: Yb^{3+} nanocomposites.

Fig. 3b. PL emission spectra of ZnO: Mg^{2+}: Yb^{3+} nanocomposites.

Fig. 3c. Gaussian fitting of Photoluminescence emission peak of ZnO/MgO (30%Mg, 1%Yb)

Fig. 4. Time decay luminescence curve of Yb^{3+} doped ZnO/MgO nanocomposites.

FIGURES

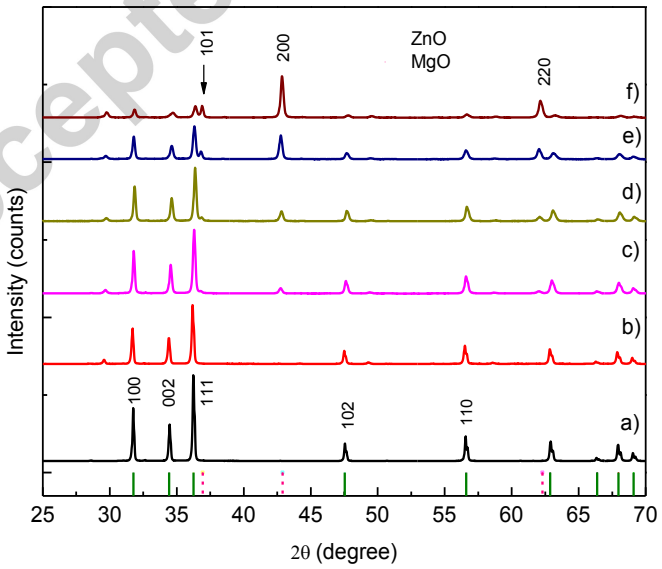

Fig. 1a. XRD pattern of Mg^{2+}: Yb^{3+}: ZnO nanophosphor powder (a) $Mg_{(5\%)}Yb_{(1\%)}$:ZnO, (b) $Mg_{(10\%)}Yb_{(1\%)}$:ZnO, (c) $Mg_{(20\%)}Yb_{(1\%)}$: ZnO, (d) $Mg_{(30\%)}Yb_{(1\%)}$:ZnO, (e) $Mg_{(50\%)}Yb_{(1\%)}$:ZnO, (f) $Mg_{(70\%)}Yb_{(1\%)}$:ZnO

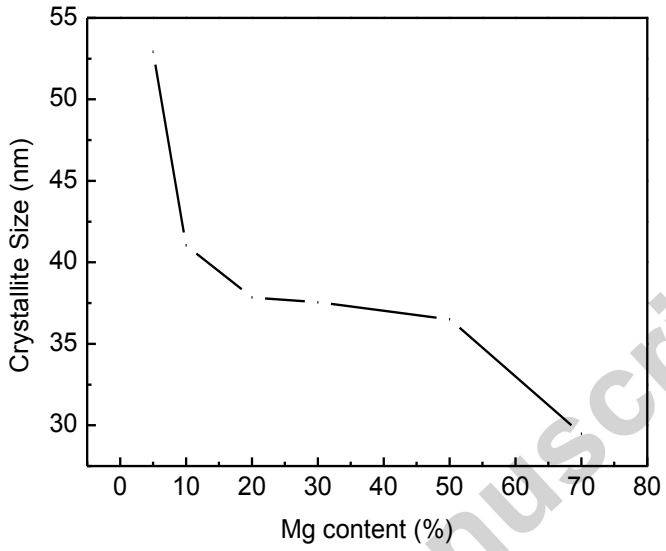

Fig. 1b. The variation of crystallite size in Yb^{3+} doped ZnO/MgO nanocomposites calculated from Scherrer equation.

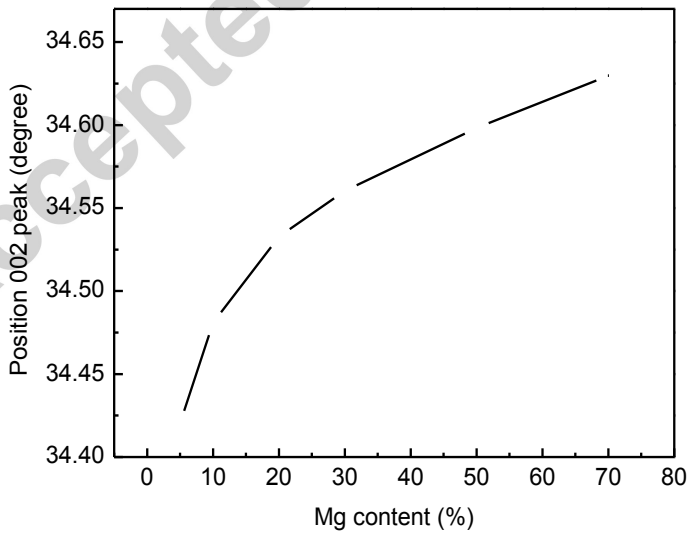

Fig. 1c: Position of 002 diffraction peak of ZnO in Yb^{3+} doped ZnO/MgO nanocomposites.

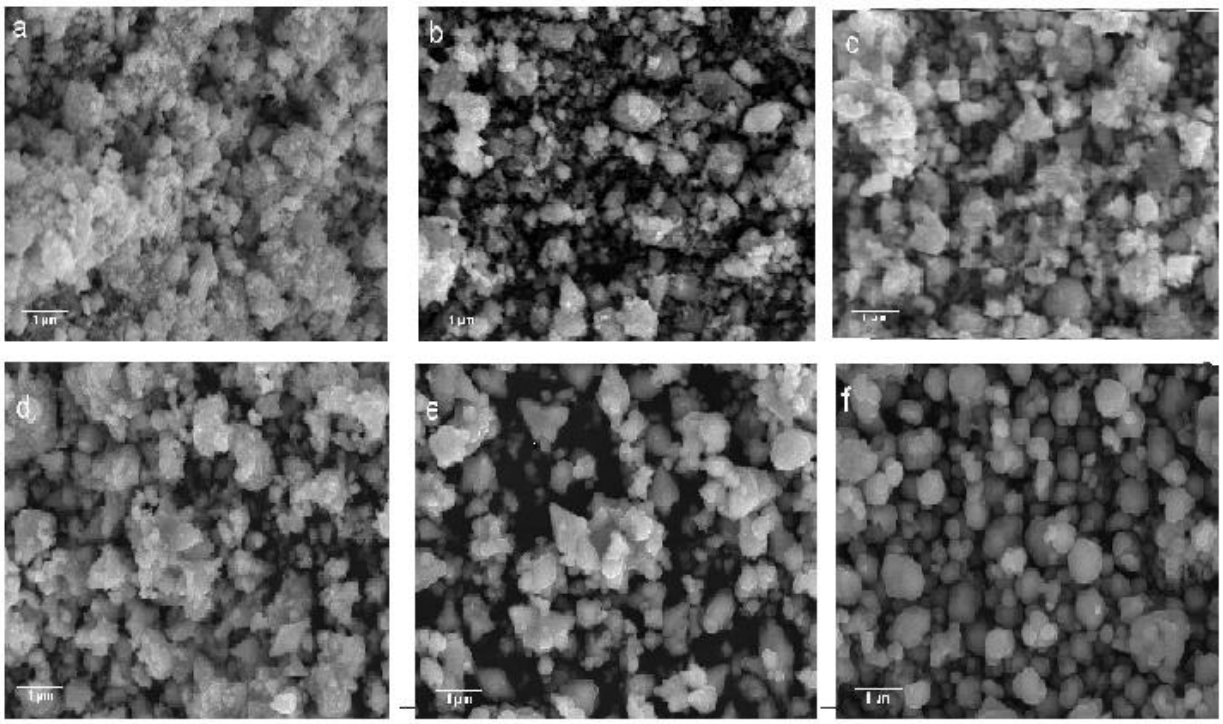

Fig.2 SEM analysis of Yb^{3+} doped ZnO/MgO nanocomposites: (a) $Mg_{(5\%)}Yb_{(1\%)}$:ZnO, (b) $Mg_{(10\%)}Yb_{(1\%)}$:ZnO, (c) $Mg_{(20\%)}Yb_{(1\%)}$: ZnO, (d) $Mg_{(30\%)}Yb_{(1\%)}$:ZnO, (e) $Mg_{(50\%)}Yb_{(1\%)}$:ZnO, (f) $Mg_{(70\%)}Yb_{(1\%)}$:ZnO.

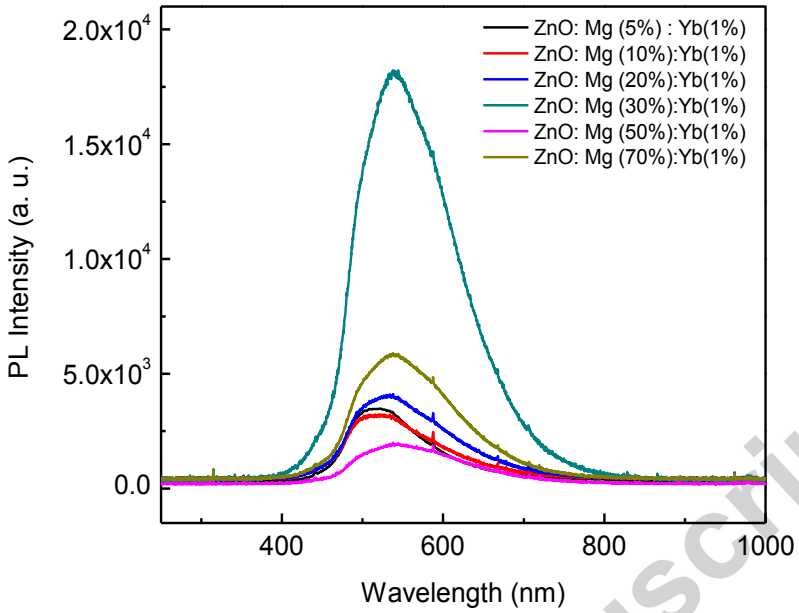

Fig. 3a. PL emission spectra ZnO: Mg^{2+}: Yb^{3+} nanocomposites

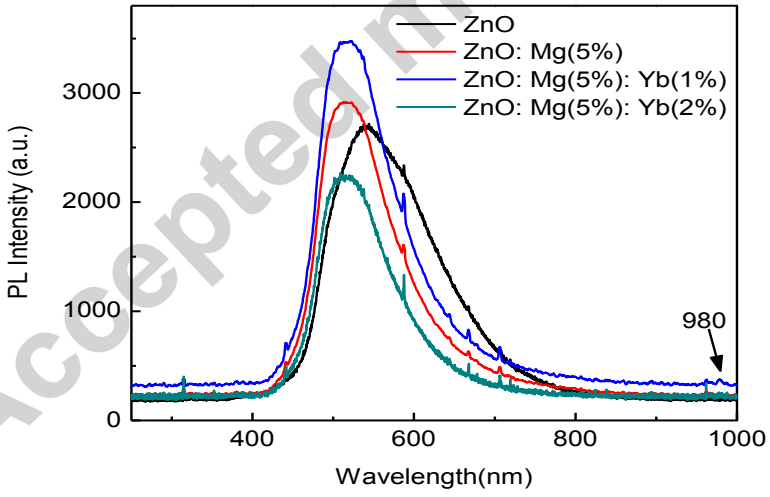

Fig. 3b. PL emission spectra of ZnO: Mg^{2+}: Yb^{3+} nanocomposites

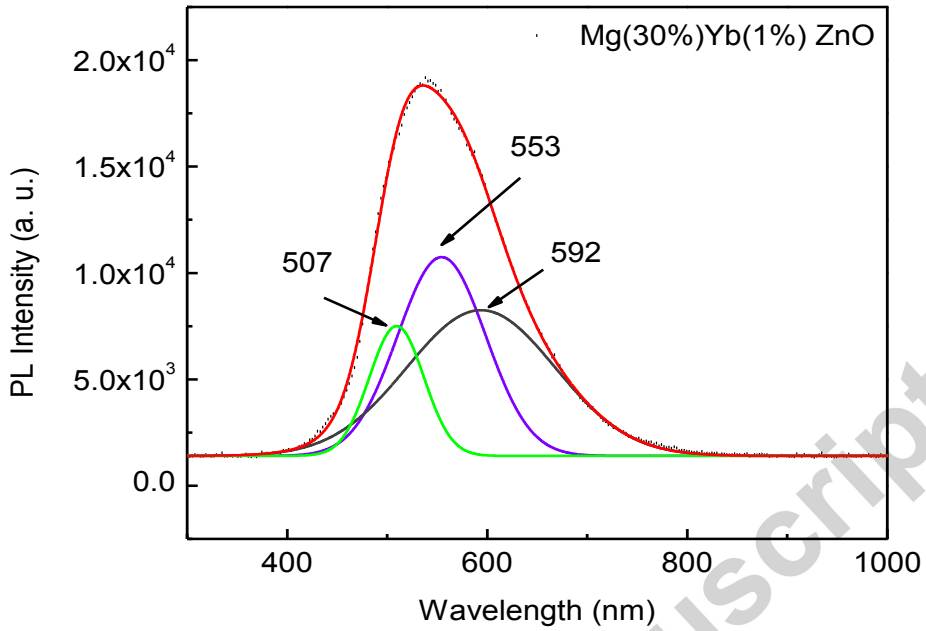

Fig. 3c. Gaussian fitting of Photoluminescence emission peak of ZnO/MgO (30%Mg, 1%Yb).

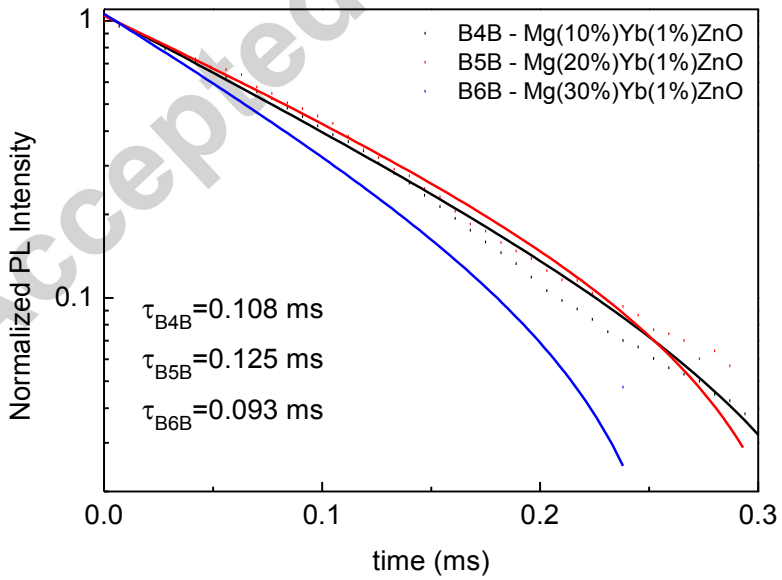

Fig. 4: Time decay luminescence curve of Yb^{3+} doped ZnO/MgO nanocomposites.

TABLES

Table 1: Stoichiometric composition and as calculated from EDAX analysis of Yb^{3+} doped ZnO/MgO nanocomposites.

		Starting composition in the initial mixture (Atomic %)					Final composition according to EDAX measurements (Atomic %)				
Sample id	Composition	O	Zn	Mg	Yb	TOTAL	O	Zn	Mg	Yb	TOTAL
B1A	Mg(5%)Yb(1%)Zn(94%)O	50	47.0	2.5	0.5	100.0	45.3	49.1	4.3	1.3	100.0
B4A	Mg(10%)Yb(1%)Zn(89%)O	50	44.5	5	0.5	100.0	48.7	42.1	7.6	1.6	100.0
B5A	Mg(20%)Yb(1%)Zn(79%)O	50	39.5	10	0.5	100.0	50.0	34.8	14.0	1.2	100.0
B6A	Mg(30%)Yb(1%)Zn(69%)O	50	34.5	15	0.5	100.0	50.4	27.7	21.1	0.8	100.0
B7A	Mg(50%)Yb(1%)Zn(49%)O	50	24.5	25	0.5	100.0	52.6	8.9	37.8	0.7	100.0
B8A	Mg(70%)Yb(1%)Zn(29%)O	50	14.5	35	0.5	100.0	51.3	6.2	42.1	0.4	100.0